Appendices

Appendix to Chapter 2

Anisotropy in molecular magnets: the g-tensor

A way to model the magnetic anisotropy of an ion is by defining the g-tensor:

$$\boldsymbol{g} = \begin{pmatrix} g_{xx} & g_{xy} & g_{xz} \\ g_{yx} & g_{yy} & g_{yz} \\ g_{zx} & g_{zy} & g_{zz} \end{pmatrix}$$

where $\boldsymbol{g}$ is a real, symmetric 3×3 matrix and therefore $g_{xy} = g_{yx}, g_{xz} = g_{zx}, g_{zy} = g_{yz}$.

The Zeeman Hamiltonian describing the interaction between the magnetic field and the effective spin operator $\vec{\mathbf{S}}'$ can be modelled using the g-tensor:

$$\boldsymbol{H_Z} = \mu_B \vec{\boldsymbol{H}} \boldsymbol{g} \vec{\boldsymbol{S}}'$$

where $\vec{\mathbf{H}}$ is the magnetic field strength and μ_B the Bohr magneton.

When possible, the procedure to compute the anisotropy tensor of a magnetic ion is to diagonalise the g-tensor. The diagonal elements will then give the direction of the anisotropy axis. In very anisotropic Kramers ions, one of the diagonal elements is much larger than the other two (usually g_{zz} by convention): $g_{zz} \gg g_{xx}, g_{yy}$.

In this case, g_{zz} is known as "easy anisotropy axis" and a magnetic field applied in this direction would yield a much higher magnetisation than if applied in the g_{xx}, g_{yy} directions.

Paramagnetic relaxation

Temperature dependence of the relaxation times for different processes

The temperature dependence of the relaxation time in an **Orbach relaxation** process is:

$$\tau = \tau_0 \exp\left(\frac{U_{eff}}{k_B T}\right)$$

where τ_0 is the characteristic length parameter, U_{eff} the anisotropy barrier, k_B Boltzmann's constant and T the temperature. Thus, if a magnetic molecule relaxes via Orbach relaxation, the anisotropy energy barrier can be determined.

The temperature dependence of the relaxation time in a **Direct relaxation** process for a Kramers ion is:

$$\tau^{-1} \propto H^4 T$$

where H is the applied magnetic field and T is the temperature. This formula is valid in the high temperature limit.

The temperature dependence of the relaxation time in a **Raman relaxation** process for a Kramers ion is:

$$\tau^{-1} \propto T^{9}$$

The derivation of the formulas in great detail can be found in reference [20].

Appendix to Chapter 3

Sample description

Distances

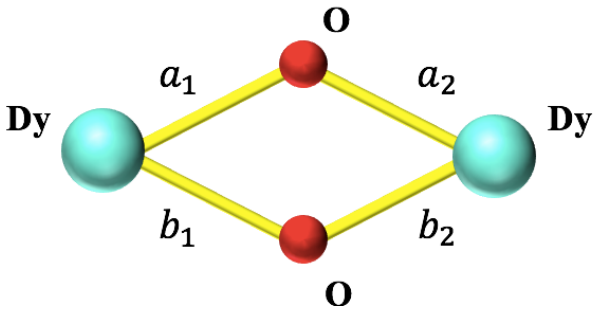

Figure A1. Definition of the distances a_1, a_2, b_1, b_2.

Molecule 2015

Ion pair	a_1(Å)	a_2(Å)	b_1(Å)	b_2(Å)	a(Å)	b(Å)	D(Å)
$Dy^{(1)}$- $Dy^{(2)}$	2,427	2,320	2,654	2,234	4,746	4,888	4,816
$Dy^{(2)}$- $Dy^{(3)}$	2,421	2,494	2,425	2,379	4,914	4,804	4,858
$Dy^{(3)}$- $Dy^{(4)}$	2,333	2,486	2,335	2,521	4,816	4,856	4,836
$Dy^{(4)}$- $Dy^{(5)}$	2,618	2,380	2,604	2,278	4,998	4,882	4,940
$Dy^{(5)}$- $Dy^{(6)}$	2,332	2,509	2,335	2,578	4,840	4,912	4,876
$Dy^{(6)}$- $Dy^{(7)}$	2,523	2,362	2,561	2,341	4,884	4,902	4,892
$Dy^{(7)}$- $Dy^{(1)}$	2,362	2,423	2,396	2,419	4,784	4,814	4,798

Table A1. Molecule 2015. Distances a_1, a_2, b_1, b_2 measured in Angstrom Å. The remaining distances are defined $a = a_1 + a_2, b = b_1 + b_2$ and $D = (a + b)/2$.

Molecule 2016

Ion pair	a_1(Å)	a_2(Å)	b_1(Å)	b_2(Å)	a(Å)	b(Å)	D(Å)
$Dy^{(1)}$- $Dy^{(2)}$	2,272	2,502	2,362	2,476	4,753	4,838	4,795
$Dy^{(2)}$- $Dy^{(3)}$	2,442	2,311	2,549	2,384	4,753	4,933	4,843
$Dy^{(3)}$- $Dy^{(4)}$	2,598	2,380	2,368	2,320	4,978	4,688	4,833
$Dy^{(4)}$- $Dy^{(5)}$	2,314	2,563	2,598	2,373	4,877	4,971	4,934
$Dy^{(5)}$- $Dy^{(6)}$	2,397	2,358	2,357	2,404	4,755	4,761	4,758
$Dy^{(6)}$- $Dy^{(7)}$	2,394	2,428	2,230	2,449	4,822	4,679	4,750
$Dy^{(7)}$- $Dy^{(1)}$	2,386	2,379	2,473	2,302	4,765	4,775	4,770
$Dy^{(3)}$- $Dy^{(5)}$	2,380	2,373			4,752		4,752

Table A2. Molecule 2016. Distances a_1, a_2, b_1, b_2 measured in Angstrom Å. The remaining distances are defined $a = a_1 + a_2, b = b_1 + b_2$ and $D = (a + b)/2$. Molecule 2015 has an extra Dy-Dy due to the single oxygen bridge.

The distances "D" are the average length of the double oxygen bridge from one Dy(III) ion to another. The distances range between $4{,}798 - 4{,}940$ Å for molecule 2015 and $4{,}752 - 4{,}934$ Å for molecule 2016, which are similar values for both molecules.

Angles

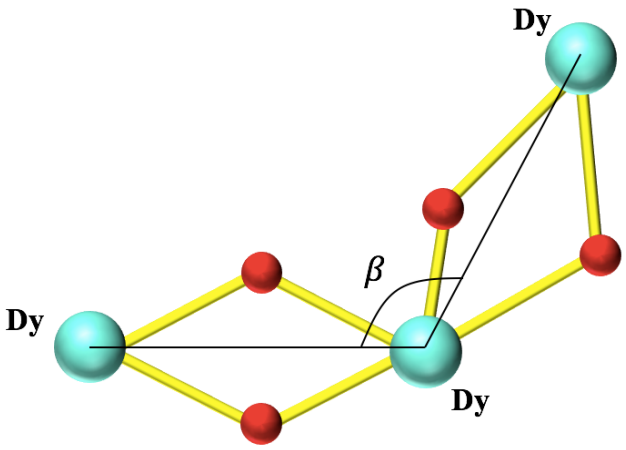

Figure A2. Definition of the angle Dy-Dy-Dy, β.

Molecule 2015

Ion trio	β(°)
$Dy^{(1)}$- $Dy^{(2)}$- $Dy^{(3)}$	116,0
$Dy^{(2)}$- $Dy^{(3)}$- $Dy^{(4)}$	91,1
$Dy^{(3)}$- $Dy^{(4)}$- $Dy^{(5)}$	119,6
$Dy^{(4)}$- $Dy^{(5)}$- $Dy^{(6)}$	122,4
$Dy^{(5)}$- $Dy^{(6)}$- $Dy^{(7)}$	114,4
$Dy^{(6)}$- $Dy^{(7)}$- $Dy^{(1)}$	95,6
$Dy^{(7)}$- $Dy^{(1)}$- $Dy^{(2)}$	117,4

Molecule 2016

Ion trio	β(°)
$Dy^{(1)}$- $Dy^{(2)}$- $Dy^{(3)}$	117,3
$Dy^{(2)}$- $Dy^{(3)}$- $Dy^{(4)}$	98,3
$Dy^{(3)}$- $Dy^{(4)}$- $Dy^{(5)}$	70,6
$Dy^{(4)}$- $Dy^{(5)}$- $Dy^{(6)}$	111,9
$Dy^{(5)}$- $Dy^{(6)}$- $Dy^{(7)}$	97,5
$Dy^{(6)}$- $Dy^{(7)}$- $Dy^{(1)}$	121,3
$Dy^{(7)}$- $Dy^{(1)}$- $Dy^{(2)}$	97,6

Table A3. Angles Dy-Dy-Dy as defined in Figure A2.

The angles for both molecules are similar but not identical. Molecule 2016 seems to be slightly more bent inwards than molecule 2015. The reason is thought to be the extra single oxygen bridge.

Equipment

AC magnetisation two-point measurements

In the first part of the measurement, the sample is positioned in point 1 (Figure A3), that is, at the centre of the positively oriented bottom coil. An AC magnetic field is applied so that the AC signal coming from the sample and the signal coming from the AC field are suppressed. This magnetic field is called “nulling waveform”. The second part of the two-point measurement takes place at point 2 (Figure A3), that is, at the centre of the two coils oriented in the opposite direction with respect to the coil in point 1 (negative orientation). The AC driving field and the nulling waveform are applied. The nulling waveform cancels the AC field as it did in point 1. However, since the coils are negatively oriented, the sample produces an AC signal that interferes constructively with the nulling waveform. As a result, the AC signal of the sample is increased 3-fold. Hence, the desired AC magnetisation of the sample is a third of the measured AC signal.

A more thorough explanation can be found in reference [35].

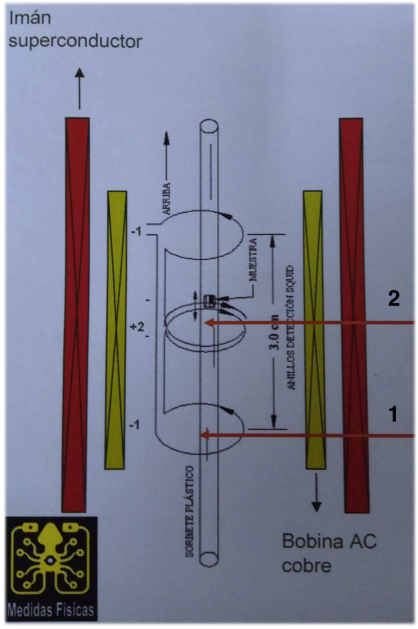

Figure A3. Depiction of the sample straw in the pickup coil. Points 1 and 2 are used in the AC measurements.

Appendix to Chapter 4

DC measurements

Derivation of the Curie-Weiss law

The interaction between magnetic centres within a molecule to derive the Curie-Weiss law is modelled in the "molecular field approximation" by introducing a perturbation in the Zeeman interaction Hamiltonian. This perturbation reads $-z\alpha < J_z > \mathbf{J_z}$ where z is the number of nearest neighbours around a magnetic centre, α is the strength of the exchange between magnetic centres and $< J_z >$ is the mean value of the z-component of the total angular momentum operator. The Zeeman Hamiltonian then reads:

$$\boldsymbol{H_Z} = g\mu_B \boldsymbol{S_z} H - z\alpha < J_z > \boldsymbol{J_z}$$

where H is the magnetic field in the z direction, the g-tensor is assumed to be isotropic and μ_B is the Bohr magneton. The eigenvalues are given by:

$$E = M_J(g\mu_B H - z\alpha < J_z >)$$

where M_J is the spin quantum number associated with $\mathbf{J_z}$.

The magnetisation M of a system may be expressed:

$$M = -Ng\mu_B < J_z >$$

where N is the number of magnetic centres.

From statistical physics, the mean value of the z-spin operator can be expressed:

$$< J >= \frac{\sum_{M_J=-J}^{J} M_J \exp\left(-\frac{E}{k_B T}\right)}{\sum_{M_J=-J}^{J} \exp\left(-\frac{E}{k_B T}\right)}$$

after solving substituting with the eigenvalues:

$$< J_z >= -\frac{J(J+1)g\mu_B H}{3k_B T - z\alpha J(J+1)}$$

Therefore:

$$M = N\frac{J(J+1)g^2\mu_B^2 H}{3k_B T - z\alpha J(J+1)}$$

Since $\chi = \mathrm{dM/dH}$:

$$\chi = N\frac{J(J+1)g^2\mu_B^2}{3k_B T - z\alpha J(J+1)}$$

And therefore, the Curie-Weiss law:

$$\chi = \frac{C}{T - \Theta}$$

with

$$\Theta = \frac{z\alpha J(J+1)}{3k_B}$$

as seen in Chapter 4. Experimental results and data treatment.

Magnetisation

Calculation of the g-tensors

The g-tensor for Dy_1 is:

$$\boldsymbol{g}^{(1)} = \begin{pmatrix} 0 & 0 & 0 \\ 0 & 0 & 0 \\ 0 & 0 & 19 \end{pmatrix}$$

The rotation matrices used to derive the rest g-tensors are:

$$R_x(\theta) = \begin{pmatrix} 1 & 0 & 0 \\ 0 & cos\theta & sen\theta \\ 0 & -sen\theta & cos\theta \end{pmatrix} \qquad R_y(\theta) = \begin{pmatrix} cos\theta & 0 & sen\theta \\ 0 & 1 & 0 \\ -sen\theta & 0 & cos\theta \end{pmatrix}$$

The g-tensor for Dy_7 was obtained by rotating $g^{(1)}$ 23° with respect to the x axis and 14 ° with respect to the y axis:

$$\boldsymbol{g}^{(7)} = R_x(23)R_y(14)g^{(1)}R_y^{-1}(14)R_x^{-1}(23)$$

The anisotropy axis for Dy_4 was observed to be very similar to that of Dy7 and therefore:

$$\boldsymbol{g}^{(4)} = g^{(7)}$$

The g-tensor for Dy_2 was obtained by rotating $g^{(7)}$ 90° with respect to the x axis:

$$\boldsymbol{g}^{(2)} = R_x(90)g^{(7)}R_x^{-1}(90)$$

The g-tensor for Dy_5 was obtained by rotating $g^{(1)}$ 30° with respect to the x axis and 30° with respect to the y axis:

$$\boldsymbol{g}^{(5)} = R_x(30)R_y(30)g^{(1)}R_y^{-1}(30)R_x^{-1}(30)$$

The g-tensor for Dy_3 was obtained by rotating $g^{(1)}$ 40° with respect to the x axis and 45° with respect to the y axis:

$$\boldsymbol{g}^{(3)} = R_x(40)R_y(45)g^{(1)}R_y^{-1}(45)R_x^{-1}(40)$$

The g-tensor for Dy_6 was obtained by rotating $g^{(1)}$ 42° with respect to the x axis and 37° with respect to the y axis:

$$\boldsymbol{g}^{(6)} = R_x(42)R_y(37)g^{(1)}R_y^{-1}(37)R_x^{-1}(42)$$

The calculated g-tensors are presented in the following subsection (Table A4).

Comparison of M(H) for both molecules

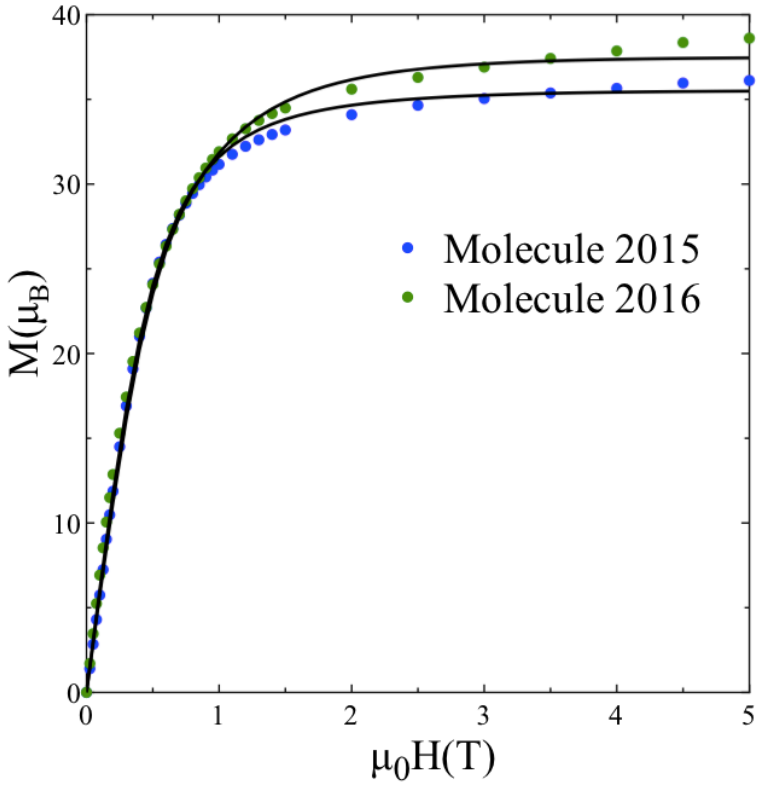

Figure A4. Comparison of M(H) curves for both molecules. The black curves are the simulations.

Table of anisotropy tensor elements

Ion	g_{xx}	g_{xy}	g_{xz}	g_{yx}	g_{yy}	g_{yz}	g_{zx}	g_{zy}	g_{zz}
$Dy^{(1)}$	0,0	0,0	0,0	0,0	0,0	0,0	0,0	0,0	19,0
$Dy^{(2)}$	0,95	3,8	-1,6	-3,8	15,2	-6,6	-1,6	6,6	2,8
$Dy^{(3)}$	5,6	-6,5	5,6	-6,5	7,9	-6,5	9,6	-6,5	5,6
$Dy^{(4)}$	0,95	-1,6	3,8	-1,6	2,8	6,6	3,8	6,6	15,2
$Dy^{(5)}$	3,5	-4,0	-6,2	-4,0	4,75	-4,0	6,2	-4,0	10,6
$Dy^{(6)}$	3,8	-5,6	5	-5,6	8,5	-7,5	5	-7,5	6,6
$Dy^{(7)}$	0,95	-1,6	3,8	-1,6	2,8	6,6	3,8	6,6	15,2

Table A4. Calculated components of the g-tensor elements for each Dy(III) ion. The highlighted data are inputs to the simulation programme.

How are the g-tensors affected by small variation in the rotation angles?

The g-tensor for Dy_1 is:

$$g^{(1)} = \begin{pmatrix} 0 & 0 & 0 \\ 0 & 0 & 0 \\ 0 & 0 & 19 \end{pmatrix}$$

If the anisotropy axis for Dy_7 was rotated as little as 10° with respect to the y axis, $\boldsymbol{g}^{(7)}$ would read:

$$\boldsymbol{g}^{(7)} = \begin{pmatrix} 0{,}55 & 0 & 3{,}1 \\ 0 & 0 & 0 \\ 3{,}1 & 0 & 18{,}2 \end{pmatrix}$$

which has non-negligible off-diagonal components: $\frac{3{,}1}{18{,}2} \approx 17\%$.

This result implies that small inaccuracies in estimating the angles that the anisotropy axes of the Dy(III) ions form with the x, y and z axes will lead to big differences in the g-tensors. This is relevant since the programme used for the simulation of M(H) does not take off-diagonal components.

AC susceptibility measurements

Fitting comparisons: 1 relaxation time versus 2 relaxation times for molecule 2016

An attempt to fit the data curves with two relaxation parameters was only possible for a DC field of $H_{DC} = 1500$ Oe; Figure A5:

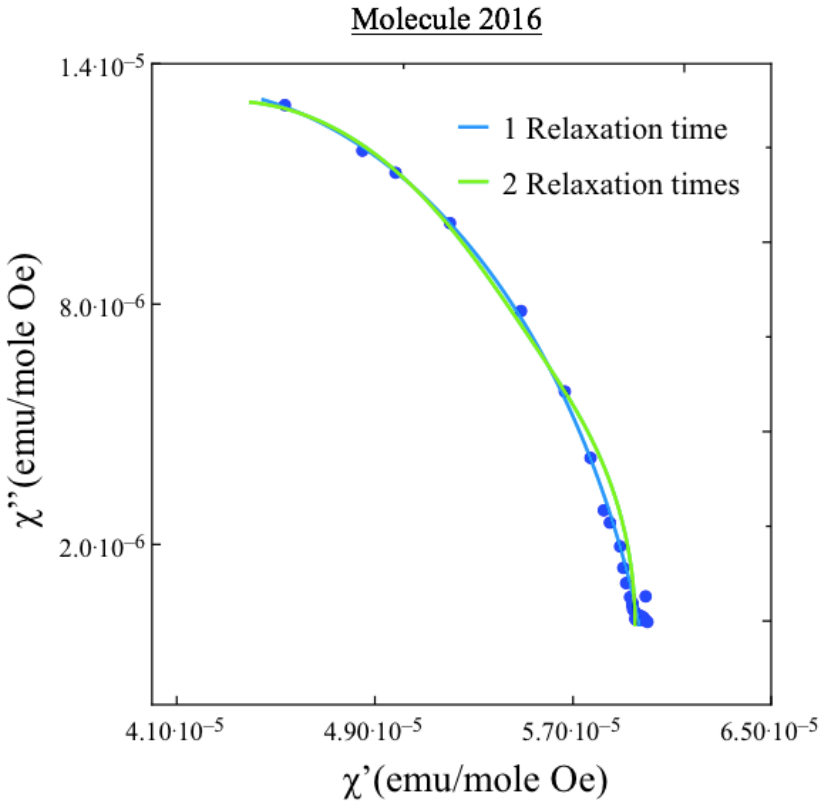

Figure A5. Molecule 2016. AC susceptibility curves for $H_{DC} = 1500$ Oe. The green fitting corresponds to 2 relaxation times and the blue to 1 relaxation time.

The fitting to 2 relaxation parameters deviates more from the experimental data than the fitting for one relaxation parameter. Thus, the fitting to one relaxation time proves to be best.

Tables

$H_{DC}(Oe)$	$\tau\ (ms)$	$\Delta\tau\ (ms)$	α	$\Delta\alpha$
0	0,048	0,065	0,38	0,05
500	0,33	0,042	0,18	0,02
750	0,42	0,022	0,18	0,01
1500	0,49	0,020	0,21	0,01
2500	0,59	0,029	0,25	0,01
3500	0,55	0,025	0,32	0,01
5000	0,55	0,067	0,39	0,01
10000	1,16	0,044	0,41	0,05

Table A5. Molecule 2016. Fitted values of τ and α with their respective fitting uncertainties Δτ and Δα for different DC fields at c.

$T(K)$	$\tau_1\ (ms)$	$\Delta\tau_1\ (ms)$	α	$\Delta\alpha$
1.8	0,51	0,014	0,2	0,01
2.3	0,40	0,017	0,18	0,01
2.8	0,32	0,012	0,18	0,01
3.3	0,26	0,012	0,18	0,01
3.8	0,24	0,014	0,18	0,01
4.3	0,20	0,010	0,18	0,01
5	0,17	0,012	0,18	0,01

Table A6. Molecule 2016. Fitted values of τ and α with their respective fitting uncertainties Δτ and Δα at different temperatures for a fixed field of $H_{DC} = 1500$ Oe.

$H_{DC}\ (Oe)$	$\tau_1\ (ms)$	$\Delta\tau_1\ (ms)$	$\tau_2\ (ms)$	$\Delta\tau_2\ (ms)$	$\tau_3\ (s)$	$\Delta\tau_3\ (s)$
0	0,75	0,21	10,9	4,1		
300	0,21	0,025	5,1	1,5		
800	0,43	0,062	5,8	1,6	5,00	2,3
1200	0,59	0,17	12,6	5,9	5,52	0,91
2000	0,92	0,40	55,0	3,1	8,36	0,26
3500	0,95	0,2	101,0	25,2	8,03	0,45
5000	0,73	0,08	81,6	8,7	6,72	0,18
10000	0,48	0,13	77,1	72,8	4,27	0,92

Table A7. Molecule 2015. Relaxation times and their respective uncertainties for different DC fields at T = 1,8 K.

$H_{DC}\,(Oe)$	α_1	$\Delta\alpha_1$	α_2	$\Delta\alpha_2$	α_3	$\Delta\alpha_3$
0	0,41	0,03	0	0		
300	0,2	0,13	0,19	0,05		
800	0,29	0,15	0,23	0,06	0	0
1200	0,42	0,1	0,29	0,13	0	0
2000	0,53	0,1	0	0	0,14	0,05
3500	0,46	0,13	0,31	0,1	0,06	0,05
5000	0,29	0,07	0,41	0,03	0,05	0,02
10000	0,37	0,9	0,32	0,3	0	0

Table A8. Molecule 2015. Fitted values of the Cole-Cole parameters and their uncertainties for the three relaxation mechanisms.

$T(K)$	$\tau_1\,(ms)$	$\Delta\tau_1\,(ms)$	$\tau_2\,(ms)$	$\Delta\tau_2\,(ms)$	$\tau_3\,(s)$	$\Delta\tau_3\,(s)$
1,8	0,60	0,09	51,8	6,6	7.33	0.19
1,98	0,56	0,13	53,6	11,2	6.06	0.12
2,2	0,57	0,07	78,1	8,5	5.39	0.050
2,47	0,56	0,14	69,8	16,0	4.67	0.10
2,83	0,49	0,13	93,0	22,2	3.78	0.070
3,3	0,52	0,10	89,3	17,6	3.15	0.050
3,97	0,63	0,20	110,9	29,2	2.63	0.083
4,97	0,82	0,57	57,2	25,2	2.38	0.35
6,63	0,82	0,12	31,9	2,7	2.71	0.23

Table A9. Molecule 2015. Temperature variation of the relaxation times and their uncertainty.